



Drip irrigation wetting patterns and nitrate distribution: comparison between electrical resistivity (ERI), dye tracer, and 2D soil–water modelling approaches

Marcus Hardie¹ · James Ridges¹ · Nigel Swarts¹ · Dugald Close¹

Received: 19 February 2017 / Accepted: 17 December 2017 / Published online: 5 January 2018
© Springer-Verlag GmbH Germany, part of Springer Nature 2018

Abstract

Despite the widespread use of drip irrigation and fertigation, there is limited research on soil wetting patterns and nutrient distribution from drip emitters in agricultural soils. We compared the use of electrical resistivity imaging (ERI) with dye tracer patterns, measured soil nitrate distribution, and modelled changes in soil moisture and nitrate distribution, in a commercial apple orchard in southern Tasmania. Time-lapse two-dimensional ERI revealed wetting plumes beneath the emitters ranged from nil infiltration, to infiltration beyond 1.0 m depth. Lack of infiltration beneath some emitters was attributed to runoff caused by either water repellence or the surface leaf mulch, whilst infiltration to 1.0 m depth was attributed to preferential flow processes. The uncalibrated ERT was unable to discern the separate contributions from of solute concentration, moisture content and temperature to the change in electrical resistivity. The dye tracer study revealed the majority of the fertigated nitrate was retained in the A1 horizon, whilst the fertigated water infiltrated much deeper into the A2 and B2 horizons. The 2D modelling was not able to replicate the variations in infiltration demonstrated by the ERT, principally due to the lumped nature of the soil parameterisation, and inability of the model to simulate preferential flow. As such, use of modelling tools and texture-based guidelines for design and management of drip emitters is not recommended for the texture contrast soils.

Introduction

Drip fertigation involves the application of soluble nutrients through drip irrigation emitters. It is regarded as a precise and efficient method of supplying water and nutrients to crops, specifically perennial tree crops. Drip irrigation offers a large degree of control, enabling timely and precise placement of irrigation and nutrients to meet crop requirements, thereby minimising application to non-target areas and leaching of nutrients beneath the root zone (Gårdenäs et al. 2005; Thorburn et al. 2003). The shape of the wetted soil volume and nitrate distribution beneath emitters is influenced by factors such as; soil hydraulic properties, emitter discharge rates, emitter spacing, irrigation quantity and frequency, crop water uptake rates and root distribution

(Gårdenäs et al. 2005; Naglič et al. 2014; Souza and Folegatti 2008; Subbaiah 2013).

Despite the wide spread use of drip irrigation and fertigation systems in many agricultural industries, there are relatively few studies which have measured soil water and nutrient distribution following fertigation in in situ agricultural soils (Klein and Spieler 1987). Instead, guidelines for the design and operation of drip irrigation systems (FAO 1997; Goldy 2012; Hung 1995) have been developed for generic soil texture classes (e.g., sand, loam, clay) which require modification by system designers and farmers to account for local conditions (Thorburn et al. 2003). These guidelines typically present soils as being uniform in which water and nutrients infiltrate in a three-dimensional flow pattern about the dripper (Klein et al. 1989). Consequently these guidelines typically ignore many of the complexities associated with infiltration into in situ soils, including; compaction, surface crusting, and preferential flows resulting from water repellence, macroporosity, and contrasting soil horizons (Bar-Yosef et al. 1988; Flury et al. 1994; Gerke et al. 2010; Jarvis 2007). The occurrence of preferential flow is especially important with drip irrigation systems, as localized ponding beneath emitters may facilitate infiltration

Communicated by N. Lazarovitch.

✉ Marcus Hardie
marcus.hardie@utas.edu.au

¹ Perennial Horticulture Centre, Tasmanian Institute of Agriculture, University of Tasmania, Private Bag 98, Hobart, TAS 7001, Australia

through surface connected macropores, shrinkage cracks and the development of finger flow (Clothier et al. 2008; Cote et al. 2003; Roth 2008).

Strategic and tactical management of drip irrigation and fertigation systems requires the ability to rapidly and non-destructively determine emitter wetting patterns (Devasirvatham 2009; Thorburn et al. 2003). Manual determination of emitter wetting patterns following infiltration such as auguring or excavation are time consuming and result in damage to tree roots. Over the last two decades development of 2D soil water models and availability of geophysical proximal sensors has enabled non-destructive or minimally destructive means of predicting or inferring drip emitter wetting patterns and solute distribution (Samouëlian et al. 2005; Satriani et al. 2015; Subbaiah 2013).

A number of minimally invasive geophysical tools have been used to ‘map’ or spatially infer irrigation wetting patterns and solute distribution from drip emitters. Approaches include; electromagnetic induction (EM 38) (Coppola et al. 2016; Hossain et al. 2010; Misra and Padhi 2014), cosmic ray sensors (Han et al. 2016; Zhu et al. 2014), ground penetrating radar (Algeo et al. 2016; Satriani et al. 2015; Shamir et al. 2016), and electrical resistivity imaging (ERI) (Cassiani et al. 2015, 2016; Consoli et al. 2017; Michot et al. 2003; Moreno et al. 2015; Persson et al. 2015; Puy et al. 2016; Wehrer and Slater 2015). ERI or electrical resistivity tomography (ERT) produces 2D or cross section images of the soils resistance to the flow of electricity. Resistivity is influenced by soil texture, mineralogy, porosity, water content, solute concentration and temperature (Samouëlian et al. 2005). Time-lapse ERI before and after irrigation or fertigation events is therefore able to determine lumped spatial–temporal changes in soil moisture, solute concentration and soil temperature at a range of scales (Miller et al. 2008; Wehrer and Slater 2015).

Two-dimensional soil water modelling tools such as Hydrus-2D (Šimůnek et al. 2016) and WETUP (Cook et al. 2003; Kandelous and Šimůnek 2010) also have the ability to predict emitter wetting patterns and solute distribution under a wide range of soil types and management conditions. Kandelous and Šimůnek (2010) compared the ability of different modelling approaches for simulating surface and subsurface drip emitter patterns, they concluded that ‘Hydrus-2D provides good predictions and should be selected over the other models’ they evaluated. Hydrus-2D uses numerical methods to solve the Richards’ equation for variably saturated water flow, the convection–dispersion equation for solute transport in the liquid phase and diffusion equations for solute transport in the vapor phase (Šimůnek et al. 2008, 2012, 2013; Šimůnek and van Genuchten 2007). Hydrus-2D has been successfully used to model fertigation and drip irrigation practices including; Cook et al. (2006a); El-Nesr et al. (2014); Li et al. (2015); Mguidiche et al. (2015); Naglič

et al. (2014); Phogat et al. (2013); Phogat et al. (2014); Wang et al. (2014), however, its application in in situ soils is somewhat limited by difficulty parameterizing spatial–temporal variation in soil properties and limited ability to simulate preferential flow processes (Gerke et al. 2010; Šimůnek et al. 2003).

In Tasmania, approximately 26% of perennial horticulture (apples, cherries, vines) are located on texture contrast (TCS) or duplex soils (Cotching et al. 2009). These soils consist of a shallow sand to sandy loam topsoil over a clay subsoil. Infiltration into the TCS is often complex involving a number of preferential flow processes including; water repellence based finger flow, bypass flow through shrinkage cracks and macropores, and subsurface lateral flow above the A2 or B2 horizons (Chittleborough et al. 1994; Eastham et al. 2000; Hardie et al. 2013). Drip fertigation and irrigation into TCS is therefore expected to result in uneven, spatially heterogeneous, and largely unpredictable wetting patterns, as demonstrated by Hardie et al. (2012). This has important implications on irrigation and fertigation efficiency and effectiveness in commercial orchards, where the majority of nutrients are supplied by drip emitters.

This study was established in a commercial apple orchard growing on a texture contrast soils to:

1. Test the use of commercially available ERI tools for rapid non-destructive ‘mapping’ of fertigation infiltration patterns.
2. Compare fertigation infiltration patterns inferred by ERI to those predicted by Hydrus-2D, and to in situ measured values.
3. Determine the spatial distribution of irrigation and nitrate following fertigation.
4. Report the efficiency and effectiveness of a single drip fertigation and irrigation event.

Materials and methods

Field site characteristics

Location and climate

The trial was located in a commercial apple orchard within the Huon Valley, Tasmania, Australia (42°59′36.97″S, 147°59′29.04″E). The region has a temperate, maritime climate with an average rainfall of 745 mm, mean minimum and maximum temperature range of 5.8–17.1 °C, and mean daily sunshine hours of 5.5 h (BOM 2015). The orchard consisted of 10-year-old ‘Galaxy’ trees, grown on M26 rootstock, pruned to a central leader training system, with 2 m tree spacing, and 4.5 m row spacing, on a 0.3 m high

mounded tree row. The orchard had previously been irrigated by 2.3 L h⁻¹ emitters spaced every 0.5 m along the tree line.

Soil properties

Prior to trial establishment, a handheld 4 m by 20 m electromagnetic induction survey (EM) was conducted using a Geonics EM38 in QP mode, and Garmin 12 XL GPS, to locate the trial in an area of relatively homogenous soils. Apparent conductivity maps were produced using SURFER version 8, employing default kriging settings and a low level of contour smoothing. The trial was located within an area in which the apparent conductivity varied from 5 to 9 mS cm⁻¹.

Soils were classified according to Isbell (2002) as Grey, Eutrophic, Humose–Bleached Kurosol (texture contrast), which consisted of a reworked A1 (0–0.30 m) sandy loam, over a rigid bleached silica cemented A2e horizon, and a mottled carbon rich (5.19%) light clay B21 horizon, over a mottled medium clay B22 horizon. Selected soil properties are presented in Table 1. Chemical analysis was conducted by CSBP laboratories, Western Australia according to Raymond and Higginson (1992).

Soil physical analysis

Soil core samples (5.0 cm × 5.2 cm and 6.0 cm × 9.0 cm) were collected in triplicate from each soil horizon for analysis of hydrological properties. Bulk density was determined at saturation using 5.0 cm × 5.2 cm cores according to McKenzie et al. (2002). Saturated hydraulic conductivity (K_{sat}) was determined on the 5.0 cm × 5.2 cm cores by Darcy's Law at a constant head of +0.1 kPa. The soil water

release curve was determined using the 6.0 × 9.0 cm cores by evaporative flux (Peters and Durner 2008; Wendroth et al. 1993) using HYPROP apparatus and tensioVIEW software (UMS 2013). The soil water retention curve was fitted using the bimodal (dual porosity) van Genuchten–Mualem equation (Durner 1994), which better represents macroporosity than the traditional van Genuchten–Mualem equation. Parameter values are presented in Table 1.

Fertigation and irrigation experiment

Fertigation and irrigation

The trial occurred over 4 days in February, 2013. Fertigation was conducted through Netafim 15–30 kPa pressure compensating emitters at 15 kPa with a solution of calcium nitrate (4.8 g L⁻¹) and dye tracer FCF Brilliant Blue (7.0 g L⁻¹). The dye tracer was added to the fertigation water to enable visualisation of infiltration pathways into the soil, and to guide soil sampling. Irrigation (0.2 dS/m) was conducted 20 h after fertigation through the existing farm 2.3 L h⁻¹ irrigation emitters spaced at 0.5 m. High and low irrigation treatments were established in two adjacent 8.0 m long sections along a single tree row, each containing four trees. The low rate irrigation treatment was irrigated for 45 min, whilst the high irrigation rate treatment was irrigated for 90 min.

Electrical resistivity imaging

Two-dimensional electrical resistivity imaging (ERI) was conducted using a Wenner-alpha electrode array, which are highly sensitive to vertical variations in electrical

Table 1 Selected soil data

Soil horizon	Depth (cm)	Texture	Organic carbon (%)	EC _{1:5} (dS/m)	pH (CaCl ₂)	CEC (meq/100 g)	K_{sat} (mm/h)	Bulk density (g/cm ³)
Chemical and physical properties								
A1	0–30	Sandy loam	3.46	0.17	5.4	19.13	44	1.10
A2	30–50	Loamy sand	0.47	0.19	4.1	2.64	8.2	1.50
B21	50–70	Light clay	5.19	0.25	3.4	11.73	1.2	1.14
B22	70+	Medium clay	2.47	0.18	4.0	4.57	0.5	1.27
Soil horizon	Θ_r (cm/cm)	Θ_s (cm/cm)	α_1 (1/cm)	η_1	ω_2	α_2 (1/cm)	η_2	RMSE
Bimodal Durner van Genuchten–Mualem parameters								
A1	0.001	0.61	0.045	2.11	0.85	0.0071	1.16	0.0013
A2	0.11	0.34	0.020	1.57	0.29	0.0008	3.78	0.0011
B21	0.10	0.65	0.026	1.14	0.71	0.0010	1.70	0.0014
B22	0.10	0.55	0.031	1.70	0.80	0.0010	1.20	0.0016

CEC cation exchange capacity, EC electrical conductivity, K_{sat} saturated hydraulic conductivity. The RMSE refers to the fit between measures $\psi(\theta)$ data pairs and the bimodal Durner van Genuchten–Mualem equation

resistivity (Furman et al. 2003). The 64 copper electrodes were inserted every 0.25 m, over a distance of 16 m, in the center of the orchard tree row that spanned the high and low irrigation treatment sections (Fig. 1). Electrodes were inserted to a depth of 0.10 m and left in place for the duration of the trial to ensure constant electrode position and contact resistance. Five ERI scans were conducted prior to excavation of the site. These occurred; (1) 2 h before fertigation, (2) 1 h after fertigation, (3) 20 h after fertigation, following which the irrigation was applied, (4) 46 h after fertigation which was also 26 h after the irrigation event, and (5) 66 h after fertigation, which was also 46 h after the irrigation event and immediately prior to excavation of the site. Data were acquired using an Allied Associated Geophysical Ltd Tigre resistivity meter at 12 levels in which measurements were repeated twice. Data acquisition typically took 110 min. The acquired apparent electrical resistivity data were inverted using the RES2DINV software version 3.59 (Loke 2010). Data were first assessed for erroneous measurements, and then inverted without temperature correction using standard least squares method and the half-cell resistivity option to improve resolution near the soil surface. Absolute error for individual inversions with up to seven iterations was between 1.3% and 1.5%.

Changes in electrical resistivity over time were determined by simultaneous time-lapse inversion in RES2DINV software version 3.59 (Loke 2010) using the ‘minimise changes’ and ‘simultaneous inversion’ options to ensure changes in model electrical resistivity were due to actual differences in electrical resistivity values, and not due to differences associated with inverting individual data sets, and to ensure that the inversion of later timesets were constrained by the first reference model. The time-constrain weight parameter was set to 1 to keep models for later time sets similar to the earlier time sets. Absolute error for time-lapse inversions were between 3.1% and 3.7%. Data are presented on a ratio basis to demonstrate relative change in moisture and or solute, and or temperature over time.

Dye tracer

Soil pits were excavated along the center of the tree row to a depth of 1.2 m in each of the two treatments 68–72 h after fertigation. Each pit revealed dye stained infiltration pathways beneath a single emitter in each of the two irrigation treatments (shown as the photographed area in Fig. 1). Both of the dye tracer stained infiltration pathways were photographed using a Cannon 200D SLR at 21 mm focal length. Images contained a large square metal scaled border to facilitate correction for radial and keystone distortion in Photoshop CS6. Dye stained pixels were separated from unstained pixels by adjusting hue and saturation channels, enabling the dye tracer to be extracted from the surrounding background image in Photoshop CS6 (Hardie et al. 2011). The dye stained images were converted to binary format in Image J software (Abramoff et al. 2004).

Nitrate and soil moisture measurements

Nitrate and soil moisture sampling was conducted for each of the two emitter dye tracer experiments (location shown in Fig. 1). A 2.00×1.00 m wire mesh with 0.10×0.10 m openings was placed over the dye stained excavation beneath the two emitter experiments to guide soil sampling. Approximately 20 g samples were obtained by removing soil to a depth of 0.01 m from every second grid square (i.e., at 0.2×0.2 m spacing). Samples were split for determination of gravimetric moisture content by drying for 24 h at 105 °C, and for storage at 3 °C for later determination of nitrate. Thawed samples were homogenised by grinding, to which potassium chloride solution (2 mol L^{-1} , 0.040 L) was added and agitated for 18 h, to induce nitrate extraction. Nitrate concentration was determined by Cd–Cu reduction according to the USEPA method 353.3 using a Smart Chem Westco Scientific Instrument cadmium reactor (O’Dell 1993). Separate analysis was performed with known nitrate samples with different levels of dye tracer to confirm that the dye tracer did not interfere with the colorimetric determination of nitrate.

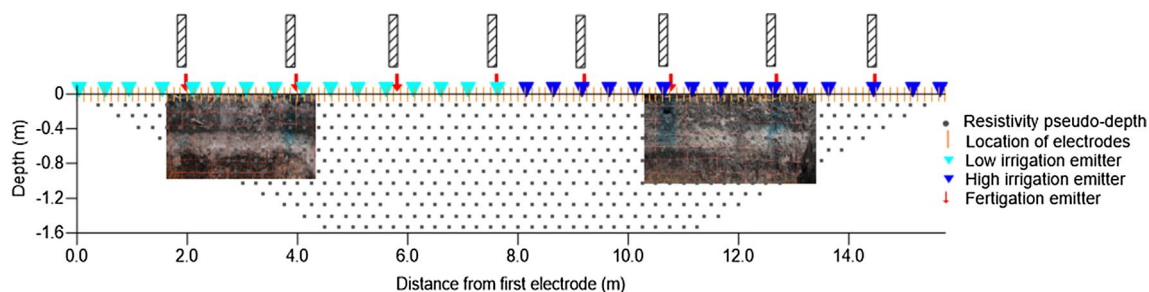


Fig. 1 Spatial representation of trial layout. Hashed bars indicate location of apple trees. Photos indicate depth and location of the two excavated dye tracers experiments, with low irrigation treatment on the left and the high irrigation treatment on the right

Nitrate and soil water modelling

Wetting patterns and solute distribution were modelled using Hydrus-2D with the bimodal (dual porosity) van Genuchten–Mualem equation (Durner 1994). The 16 m wide by 1.5 m deep experimental area was represented in a 2D vertical plane flow domain containing 5716 nodes and 10,962 elements with double the number of cells near the upper boundary. The flow domain had no-flow lateral boundaries, a free drainage lower boundary, and a no-flow upper boundary with emitters represented as time variable boundaries at 0.5 m spacings. For the two single emitter dye tracer experiments, infiltration from the emitters was simulated using the dynamic wetting option, in which the radius of the wetted area varied during infiltration, depending on the number of nodes required to maintain a negative pressure head at the soil surface (Gårdenäs et al. 2005; Naglič et al. 2014). As Hydrus-2D limits use of the dynamic wetting option to single emitters, infiltration for the 16 m long cross section experiment was simulated through a series of 0.25 m diameter circular time variable upper boundary nodes in which the number of nodes represented the width of saturated ponding beneath the emitters as indicated by the previous dynamic wetting simulations. Initial moisture contents were determined from hand auguring samples at six locations at four depths in an adjacent tree row prior to trial commencement. Representation of the spatial distribution of the four soil horizons was guided by apparent electrical resistivity and site photos. Nitrate transport was modelled using the Crank–Nicholson Scheme time weighting scheme, a longitudinal dispersivity of 5.0 cm, a transverse dispersivity of 0.5 cm and an adsorption isotherm coefficient of 0 as suggested by Gårdenäs et al. (2005). Nitrogen transformations and mineralization were not simulated due to the short duration of the experiment. As the site was covered with plastic between ERI readings, rainfall and evaporation were assumed to be zero.

Data visualization and statistical analysis

For the two excavated emitter experiments, the change in electrical resistivity 66 h after fertigation, the measured soil nitrate distribution, and the measured soil moisture were krigged and mapped as contour plots using default settings in SURFER 11 (Golden Software 2002). For the two excavated emitter experiments, statistical analysis was restricted to the soil nitrate and soil moisture sampling locations rather than krigged values. Values for the scaled TIFF layers (change in electrical resistivity, modelled soil moisture, and modelled soil nitrate) were determined by overlaying the TIFF layers with the location of the soil sampling grid, from which values for the change in electrical resistivity, modelled soil moisture, and modelled soil

nitrate were recorded. As the dye images were binary, the relationship between the presence or absence of dye tracer versus soil moisture, nitrate concentration and the change in electrical resistivity were investigated using independent *T* test in SPSS V23. Whilst the relationship between the change in electrical resistivity, soil moisture, soil nitrate concentration, modelled soil moisture, and modelled soil nitrate were explored using bivariate two tailed Pearson correlation in SPSS V23. The influence of measured and modelled soil moisture, and nitrate concentration on the change in electrical resistivity at 66 h was evaluated using stepwise linear regression with an entry probability of 0.05 in SPSS v23.

Results

Electrical resistivity imaging

The time-lapse inversion of electrical resistivity demonstrated that the change in electrical resistivity associated with infiltration beneath the emitters was highly variable (Fig. 2). The time-lapse inversion of electrical resistivity immediately and 20 h following fertigation revealed that electrical resistivity decreased (blue) beneath 5 of the 8 emitters, whilst beneath 3 of the 8 emitters the electrical resistivity had both increased (red) and decreased (blue). Changes in electrical resistivity associated with increased soil moisture and increased solute concentration following fertigation were largely restricted to the upper A1 horizon (0–0.2 m depth). However, the emitter positioned 12.8 m from the first electrode indicated that the fertigation infiltrated to at least 1.0 m depth, presumably via some form of preferential flow (Fig. 2a, b). Increased electrical resistivity (red patches, Fig. 2) between 0 and 0.2 m depth in the hour after fertigation suggests there was a slight decrease in soil moisture or solute concentration between the two ERT acquisitions. This increase in electrical resistivity was attributed to either mobilization and dilution of existing soil solutes following irrigation, or internal drainage either between the two ERT acquisitions, or during the second ERT acquisition which took 110 min. Twenty hours after fertigation (Fig. 2b) the small areas of increased electrical resistivity (red) beneath the emitters was no longer apparent, whilst the size and shape of the infiltration plumes remained mostly unchanged (Fig. 2a, b). Interestingly, in both irrigation treatments, there was no evidence of wetting associated with 3–4 emitters in the low irrigation treatment, and 3 emitters in the high irrigation treatment. All emitters were observed to be flowing during the experiment.

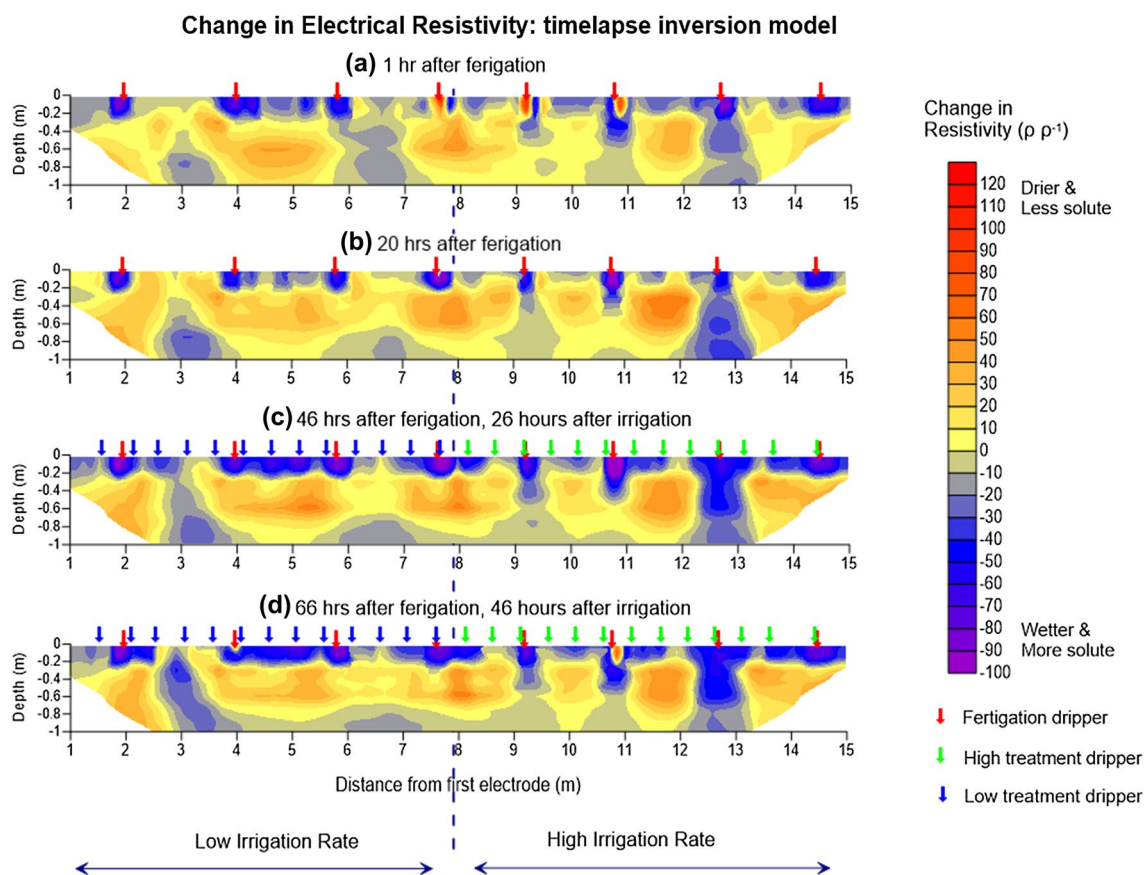


Fig. 2 Change in electrical resistivity: time-lapse inversion model demonstrating the change in electrical resistivity from the first reference model to **a** 1 h after fertigation, **b** 20 h after fertigation, **c** 46 h after fertigation and 26 h after irrigation, and **d** 66 h after fertigation and 46 h after irrigation. Dark blue arrows represent the location of

the low irrigation treatment emitters, green arrows represent the location of the high irrigation treatment emitters, red arrows indicate the location of the fertigation emitters. Left side (1.0–8.0 m) low irrigation treatment. Right side (8.0–15 m) is the high irrigation treatment. (Color figure online)

Dye tracer and nitrate distribution

For the excavated high irrigation emitter, the dye tracer wetting pattern indicated that infiltration into the A1 horizon resulted from vertical infiltration with little lateral dispersion beyond the area of ponding beneath the emitter (Fig. 3a, b). Infiltration into the A2 horizon appeared to have resulted from a combination of both lateral movement of the dye tracer along the A1/A2 horizon boundary, and non-uniform sorptive flow into the A2 horizon resulting in the appearance of finger flow. The absence of dye staining in the B22 horizon indicates little if any of the water and or solute applied during the fertigation event infiltrated into the B22 horizon (Fig. 3a, b).

In contrast to the dye tracer distribution (Fig. 3b), the nitrate was almost entirely retained within the upper A1 horizon (0–0.25 m depth) (Fig. 3c) with the majority of the nitrate retained between 0 m and approximately 0.10 m depth, with a lower concentration of nitrate extending to 0.35 m depth. Other than the low concentration

(0.02–0.04 mg g⁻¹) plume beneath 0.20 m depth, the measured soil nitrate distribution (Fig. 3c) appeared somewhat similar to that of the modelled nitrate concentration (Fig. 3g).

The change in electrical resistivity following fertigation and irrigation in the high irrigation treatment (Fig. 3e) was more uniform than either the dye tracer pattern (Fig. 3b) or the soil nitrate concentration (Fig. 3c). The change in electrical resistivity appeared as a fairly uniform band which extended to almost 0.40 m depth. As such, it appeared to be poorly related to the dye tracer distribution, soil moisture content and the nitrate distribution. The measured soil moisture distribution (Fig. 3d) appeared to be similar to the modelled soil water distribution (Fig. 3f) in which infiltration did not appear to have influenced soil moisture beyond the A1 horizon. Infiltration within the A1 horizon appeared to result from uniform flow in which the dye tracer appeared as a uniformly wetted vertical column directly beneath the ponded area beneath the emitter, as previously reported by Hardie et al. (2012).

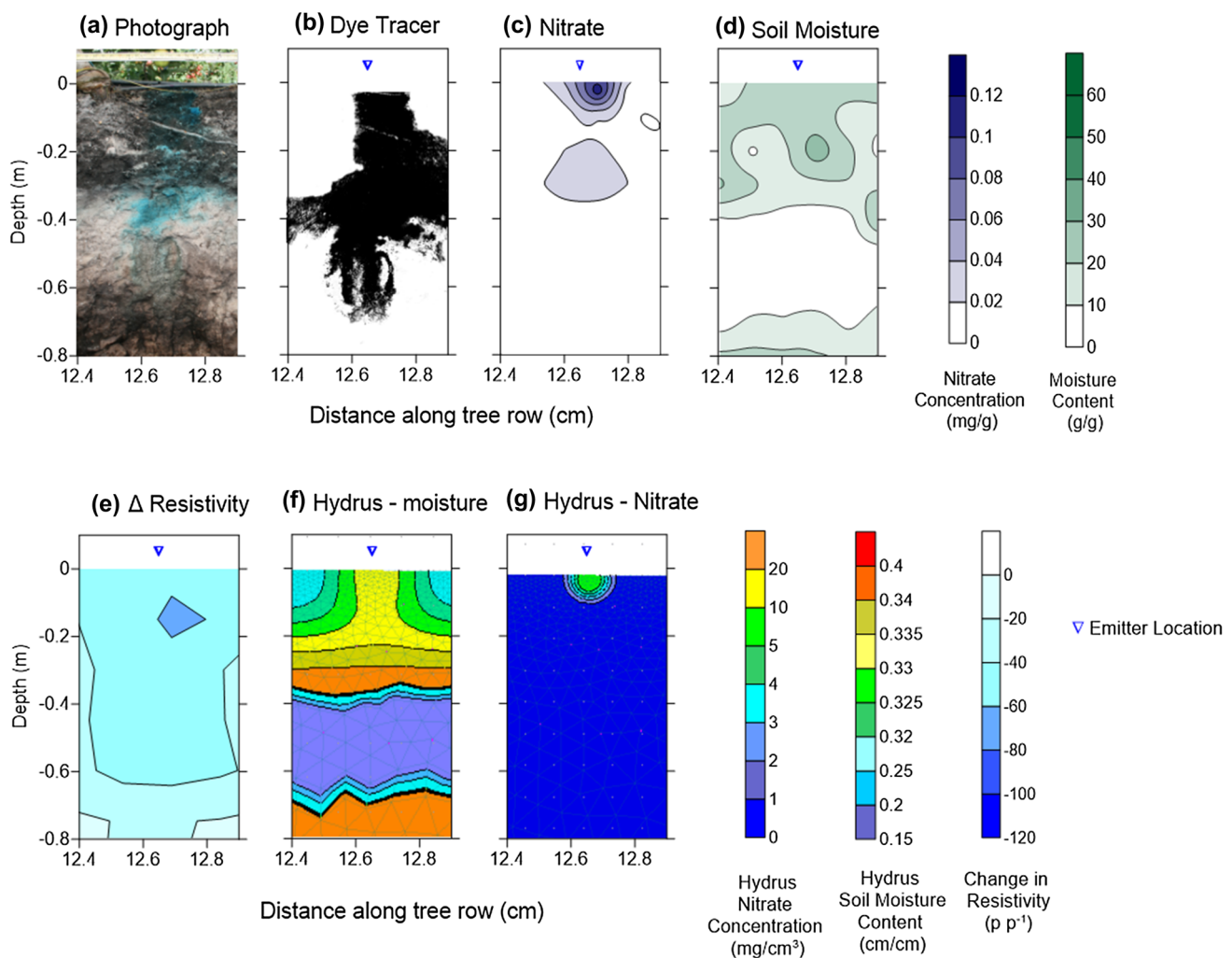


Fig. 3 Excavated emitter for the high irrigation treatment, **a** photograph of dye tracer stained soil profile, **b** extracted dye tracer pattern, **c** measured soil nitrate distribution, **d** measured soil moisture distribution, **e** ERI change in electrical resistivity 66 h after fertigation, **f**

modelled (Hydrus-2D) soil moisture 66 h after fertigation, and **g** modelled (Hydrus-2D) soil nitrate 66 h after fertigation. Triangle marks location of emitter. (Color figure online)

In the low irrigation treatment, the dye tracer pattern (Fig. 4a, b) indicated that infiltration beneath the emitter resulted from preferential flow. The dye tracer pattern (Fig. 4b) showed that the fertigation ponded beneath the emitter and spread to the left along the soil surface where it infiltrated to only 0.03 m depth. Infiltration into the soil profile then occurred as a narrow finger which broadened with depth resulting in infiltration to 0.50 m depth (Fig. 4b).

The change in electrical resistivity (Fig. 4e) appeared to show increased electrical resistivity (decreased solute and moisture) immediately beneath the dripper to a depth of approximately 0.07 m, then a broad swale of decreased electrical resistivity (increased moisture and or solute) across the soil surface to a depth of approximately 0.20 m. The nitrate distribution pattern (Fig. 4c) was similar to that of the dye tracer (Fig. 4b) in that both demonstrate spreading along the

soil surface and penetration into the near surface soil via a single narrow finger to the left of the emitter. Notably the nitrate did not penetrate as deep as the dye tracer. Unlike the high irrigation treatment, (Fig. 3c, g) in which the measured and modelled nitrate patterns appeared to be similar, in the low irrigation treatment the modelled nitrate concentration did not demonstrate spreading along the soil surface or the narrow deep infiltration through the A1 horizon (Fig. 4g).

Nitrate and soil water modelling

As expected, modelling indicated uniform and consistent infiltration of water and nitrate from each of the emitters (Fig. 5a). Twenty hours after fertigation, modelling predicted that fertigation had infiltrated to approximately 0.25 m depth, with minimal lateral dispersion away from the

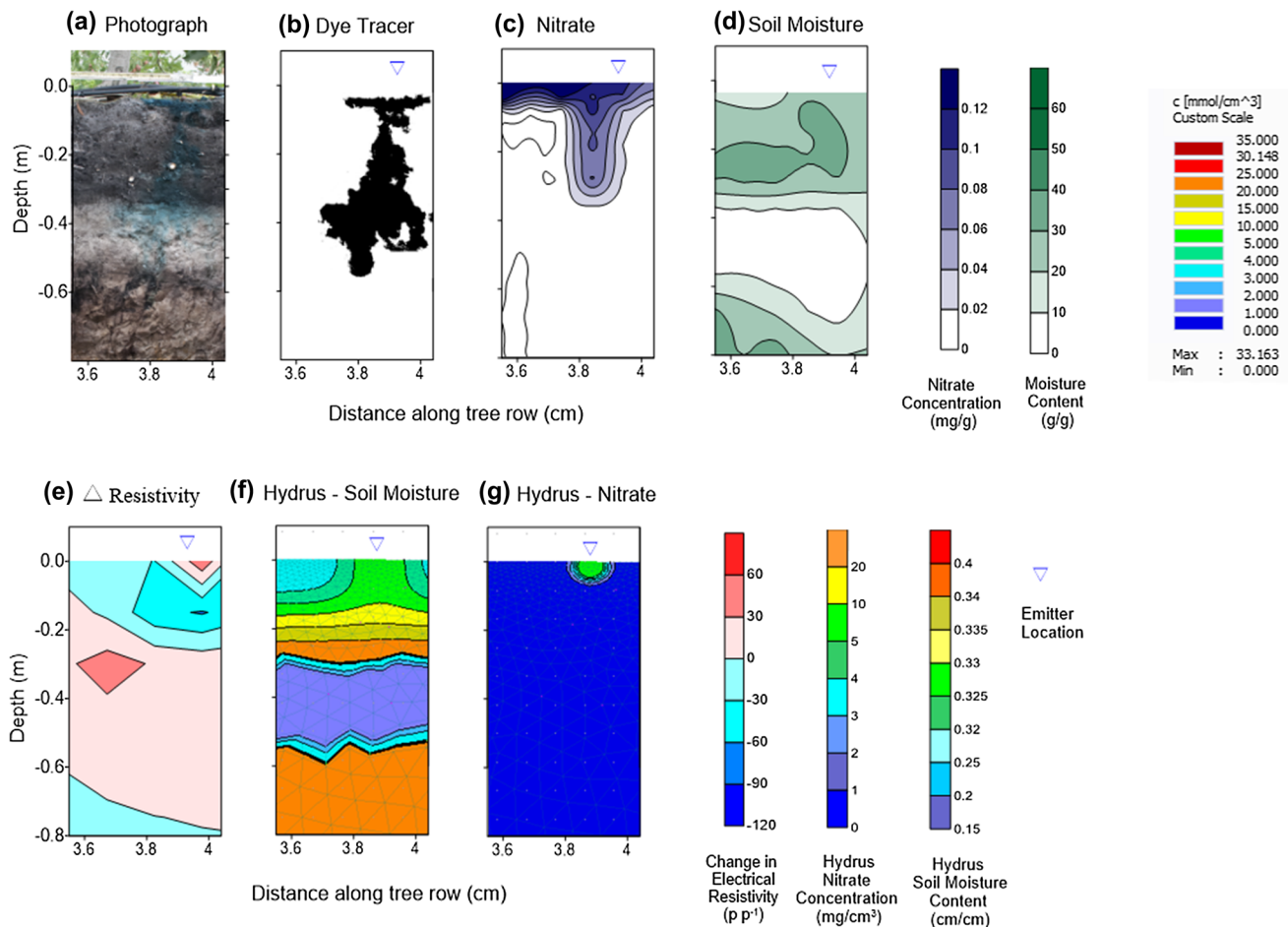


Fig. 4 Excavated emitter for the low irrigation treatment, **a** photograph of dye tracer stained soil profile, **b** extracted dye tracer pattern, **c** measured soil nitrate distribution, **d** measured soil moisture distribution, **e** ERI change in electrical resistivity 66 h after fertigation, **f**

modelled (Hydrus-2D) soil moisture 66 h after fertigation, and **g** modelled (Hydrus-2D) soil nitrate 66 h after fertigation. Blue triangle marks location of emitter. (Color figure online)

emitters (Fig. 5a). However unlike the electrical resistivity (Fig. 2), the model did not indicate fertigation infiltrated into the B2 horizons via preferential flow (Fig. 5a). In keeping with the electrical resistivity, modelling indicated a slight reduction in the moisture content in the A2 and B22 horizons as a result of internal drainage. Yet, unlike the electrical resistivity, the modelling showed a slight accumulation of water at the A2/B21 soil boundary.

Sixty-six hours after fertigation, the model indicated the low irrigation treatment resulted in infiltration to approximately 0.35 m depth, and to 0.40 m depth for the high treatment (Fig. 5b). Modelling also demonstrated that emitter spacing was sufficient to adequately wet-up the remaining A1 horizon between emitters. This finding is in contrast to the ERI which demonstrated that little if any infiltration occurred beneath up to 6 of the emitters, and

there was minimal wetting of the soil between the emitter plumes (Fig. 2c, d). Furthermore, the electrical resistivity 66 h after fertigation indicated preferential flow into the lower B22 horizon at emitters located 2.7 and 12.8 m from the first electrode, and into the A2 horizon at emitters located 9.3 and 10.8 m from the first electrode (Fig. 5a). These deeper infiltrations were not demonstrated by the model. The model indicated that the fertigated nitrate infiltrated to a depth of approximately 0.15 m depth in the area immediately beneath the emitters (Figs. 4g, 5c, d, g). Unlike the modelled soil moisture, these ‘pockets’ of nitrate remained discrete and did not form a continuous band within the A1 horizon, even after the subsequent irrigation event, which seemed to have diluted the nitrate concentration, rather than displaced the nitrate further down the soil profile (Fig. 5d).

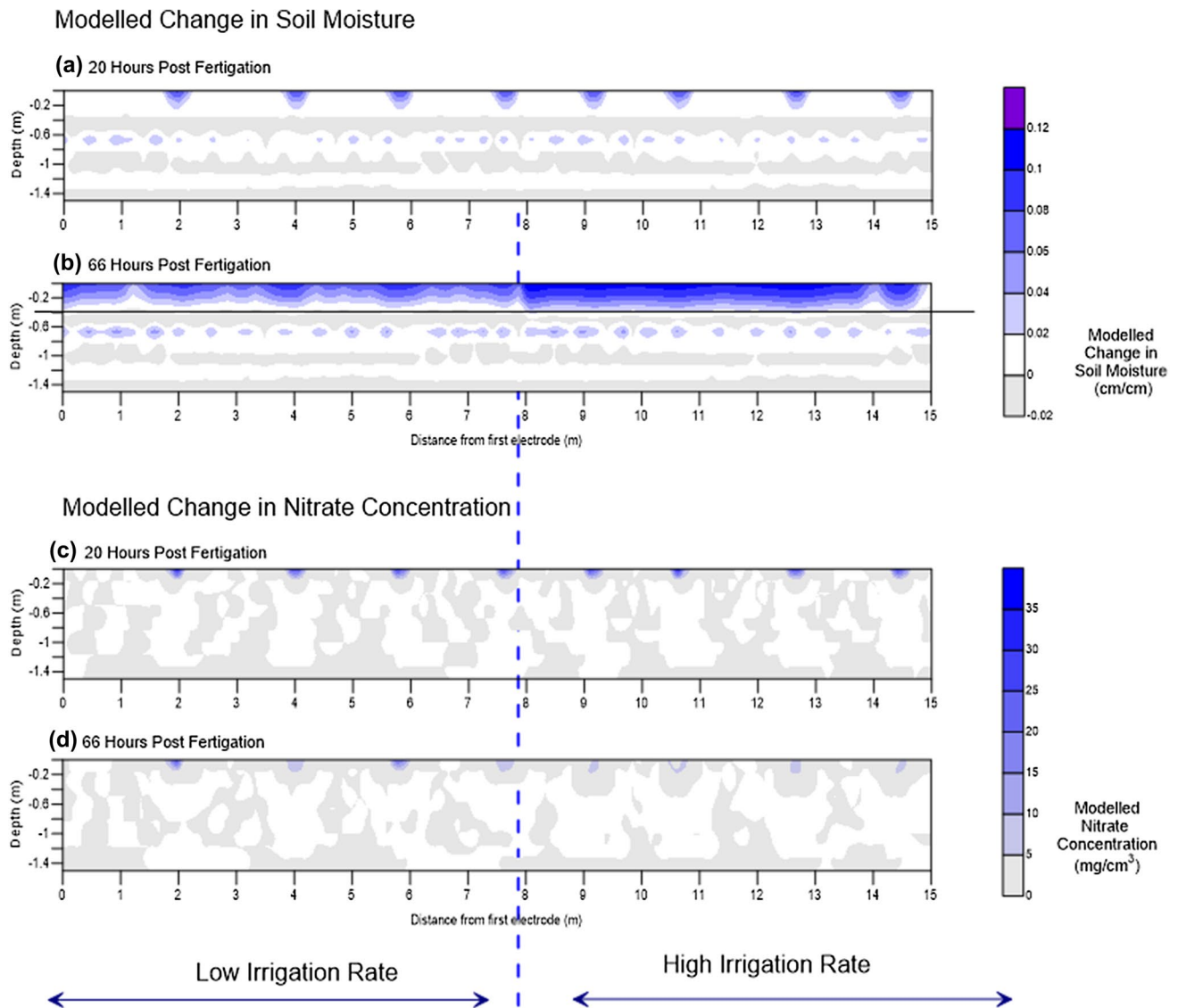


Fig. 5 Hydrus-2D modelled change in soil moisture, **a** 20 h after fertigation (before the irrigation), and **b** 66 h after fertigation. Hydrus-2D modelled nitrate concentration, **c** 20 h after fertigation (before the irrigation), and **d** 66 h after fertigation

Spatial associations between measured and modelled nitrate and soil moisture

In both irrigation treatments, the modelled soil moisture content was significantly lower ($p = 0.028, 0.001$) in the dye stained areas than in the unstained areas, the opposite of what was expected. In the high irrigation treatment, the dye stained areas had significantly ($p = 0.008$) lower change in electrical resistivity (wetter and more solute) than the unstained areas. In both the high and low treatments there was no significant difference in nitrate concentration, modelled nitrate concentration or moisture content between the dye stained and unstained areas (Table 2).

Change in electrical resistivity was significantly negatively correlated ($R^2 = 0.52, R^2 = 0.48$) with nitrate concentration in both the high and low irrigation treatments, and was significantly negatively correlated ($R^2 = 0.405$) with soil moisture, and the modelled soil moisture ($R^2 = 0.41$) in the low treatment (Table 2). The modelled soil moisture was significantly correlated with measured soil moisture in both the high and low irrigation treatments ($R^2 = 0.49, R^2 = 0.46$), and also with nitrate concentration ($R^2 = 0.283$) in the high treatment, and negatively correlated with electrical resistivity ($R^2 = 0.413$) in the low irrigation treatment (Table 2).

Multiple linear regression demonstrated that the change in electrical resistivity was most closely related to the

Table 2 Correlation between the change in electrical resistivity, measured and modelled soil moisture, and the measured and modelled nitrate distribution

	High irrigation treatment				Low irrigation treatment			
	Change in electrical resistivity	Measured nitrate concentration	Measured soil moisture	Modelled soil moisture	Change in electrical resistivity	Measured nitrate concentration	Measured soil moisture	Modelled soil moisture
Measured nitrate concentration	- 0.518**				- 0.480**			
Measured soil moisture	- 0.145	0.271*			- 0.405*	0.087		
Modelled soil moisture	0.199	0.283*	0.491**		- 0.413*	0.072	0.461**	
Modelled nitrate concentration	- 0.152	0.425**	0.244	0.107	- 0.005	0.346*	NA	- 0.016

NA not applicable, as the Hydrus solute distribution did not intersect the sampling points

*Denotes $P < 0.05$, **denotes $P < 0.001$

measured nitrate concentration (Beta = - 0.629, $P < 0.0001$: Beta = - 0.537, $P = 0.002$), followed by the modelled soil moisture (Beta = 0.392, $P = 0.001$: Beta = - 0.331, $P = 0.038$) in which the overall model fit was $R^2 = 0.41, 0.52$ for the high and low irrigation treatments respectively. No other variables were significant predictors.

Discussion

Comparison between ERI and Hydrus-2D

The ERI suggested that whilst most emitters resulted in infiltration to approximately 0.20 m depth, at two emitters infiltration penetrated to around 0.50 m depth, at a further two emitters infiltration penetrated to at least 1.0 m depth. In contrast up to 6 of the 26 emitters appeared to have had minimal if any infiltration. Checks confirmed all emitters were operating during the fertigation and irrigation events, such that we attributed the absence of infiltration beneath these 6 emitters to runoff to adjacent emitters, or runoff beyond the field of influence of the ERI due to either surface water repellence, compaction, or the presence of the surface leaf mulch. The variation in wetting patterns inferred from the ERI was somewhat greater than expected; however, drip irrigation systems are known to result in highly variable wetting patterns both horizontally and vertically (Cook et al. 2006b; Klein and Spieler 1987; Moreno et al. 2015).

The dye tracer experiments provided evidence to support findings from the ERI that infiltration beneath some of the emitters resulted from preferential flow processes. The dye tracer experiments indicated these processes to be finger flow in the A1 and A2 horizons, lateral flow along the A1/A2 soil horizon boundary, and bypass flow through shrinkage cracks and macropores in the B21 and B22 horizons.

Similar preferential flow process have been reported in texture contrast soils by Hardie et al. (2011). Finger flow usually occurs in water repellent soils as a result of instability in the wetting front (Carrillo et al. 2000; Dekker and Ritsema 1996; Ritsema et al. 1998; Wang et al. 2000a, b), however, it may also form due to compression of entrapped soil air during infiltration (Wang et al. 1997, 1998b), or unsaturated infiltration at low application rates (Wang et al. 1998a; Yao and Hendrickx 1996). In both irrigation treatments the dye tracer appeared to have moved laterally along the A1/A2 soil horizon boundary as previously reported in other Tasmanian texture contrast soils (Hardie et al. 2011, 2013) rather than above the B2 horizons as is commonly cited in the literature (Eastham et al. 2000; Ticehurst et al. 2007).

By way of comparison to the ERI, the Hydrus-2D modelling indicated infiltration was relatively uniform and consistent between emitters within each of the two irrigation rate treatments. Furthermore the modelling indicated that for both treatments, the irrigation tended to wet-up the near surface soil between each of the emitters, which was not shown by the dye tracer or ERT studies. These results suggest that even with detailed site measurements, use of lumped parameter soil water models that do not consider non-equilibrium preferential flow process are unable to predict the depth and pattern of infiltration inferred from the ERI and dye tracer studies. Whilst Hydrus-2D and a number of other models have capacity to simulate preferential flow process, these models require additional parameters which are difficult to estimate without a priori knowledge of the type and extent of preferential flows. Furthermore while spatially explicit finite element models such as Hydrus-2D are able to be parameterized at very small scales, the amount of sampling and analysis required for such parameterization would be exhaustive, destructive, and not practical for assessment of irrigation performance in commercial orchards.

Comparison between approaches at the single emitter scale

The poorer than expected correlation between the change in electrical resistivity versus moisture content and or nitrate concentration at the single emitter scale were largely attributed to differences in measurement scale between the different approaches. For example, photogrammetry was able to discern the presence or absence of the dye tracer for individual 0.4×0.4 mm pixels, compared to the change in electrical resistivity which was determined from readings 250×250 mm apart, the nitrate concentration and soil moisture which were measured on a $200 \text{ mm} \times 200 \text{ mm}$ grid, and the modelling which was conducted on cells spaced 20 mm to 50 mm apart. Koestel et al. (2009) also reported discrepancy between brilliant blue dye tracer concentration with 3D ERI, in which the ERI did not capture all the dye stained regions and underestimated sharp changes in solute concentration, which was in part attributed to the larger measurement scale of the ERI compared to the pixel size of the photographic images. Wehrer and Slater (2015) studied changes in soil moisture and solute transport in a large laboratory lysimeter using dye traces, 3D time-lapse electrical resistivity, tensiometers and capacitance soil moisture probes. They also reported that variations in water content over time were not exactly matched by the ERI, despite their ERI probes being spaced only 0.085 m apart, compared to 0.25 m in our study.

Infiltration of nitrate

Infiltration of nitrate into the A1 horizon was impeded relative to that of the dye tracer and therefore also the true wetting front. During infiltration movement of dye tracers is slower than that of the wetting front, due to absorption of the dye to soil particles, and thus the true wetting front is usually slightly ahead or deeper than indicated by dye staining patterns (Lipsius and Mooney 2006; Mon and Flury 2005). Anions such as nitrate are normally assumed to not become adsorbed by soil particles (Kowalenko and Yu 1996) and are therefore easily leached (Nováková and Nágel 2009), in which case the nitrate distribution should have been very similar to that of the wetting front and or slightly deeper than that of the dye tracer. Our findings that movement of nitrate during fertigation was impeded or moved more slowly than the infiltrating water is contradictory to expectations, but it is not unprecedented. As van der Laan et al. (2014) explains impeded movement of nitrate during infiltration may result from the presence of immobile water phases arising from the range in pore water velocities associated with the infiltrating water (Alletto et al. 2006; Clothier et al. 1995; Jarvis 2007) and or adsorption of nitrate to soil, most notably in tropical or acid soils (Kowalenko and Yu 1996).

Irrigation and fertigation efficiency

In recent years there has been growing concern about the potential for preferential flow to facilitate nitrate mobilisation to groundwater (Hu et al. 2015; Sheng et al. 2014; Smethurst et al. 2014; Williams et al. 2014). The ERI suggested that for all but two emitters, irrigation was largely restricted to the A1 and A2 horizons (approximately 0–0.40 m depth) which coincided with the highest observed root abundance at 0.30–0.35 m depth. Consequently, on a single event basis, irrigation and fertigation appeared to be highly effective and efficient. Furthermore even in the presence of preferential flows the fertigated nitrate appeared to be mostly retained in the A1 horizon. Consequently contamination risk or hazard posed by the presence of preferential flow processes transporting nitrate to shallow groundwater are somewhat less than what would otherwise be expected.

Conclusion

The ERI approach was a useful means of revealing spatial and temporal variations in infiltration patterns following drip fertigation and irrigation in a texture contrast soil. The ERI cross section demonstrated considerable variation in infiltration patterns and depth of infiltration between emitters, including infiltration to over 1.0 m depth, and no infiltration at all. These wetting patterns and those of the dye tracer differed markedly to those predicted by the model and ‘texture based’ emitter guidelines. Consequently results from this study suggest the use of ‘texture based’ emitter guidelines, and or lumped parameter soil water models are not supported for predicting emitter wetting patterns or designing irrigation systems in the texture contrast soils.

Uncalibrated use of ERI was unable to discern if changes in resistivity were due to changes in temperature, moisture or solute concentration. However simultaneous ERI, dye tracer and modelling studies revealed that changes in electrical resistivity were more strongly influenced by nitrate concentration than soil moisture content. Furthermore the dye tracer studies revealed that most of the fertigated nitrate was retained within the A1 horizon, whereas the infiltrating water penetrated through the A1 horizon, into the A2 and upper B2 horizons. Poor correlation between predicted nitrate and infiltration patterns versus and those revealed by the dye tracer and ERT studies were due to, differences in measurement scale between approaches, the limited ability of the model to simulate preferential flow process, and inability to parameterize the model at the individual emitter scale. To this end, results from this study indicate the potential to use small scale ERT surveys to improve model parameterization.

Acknowledgements The authors would like to thank the owners of the orchards for their considerable assistance during the monitoring of the orchards; Andrew Griggs of Lucaston Park Orchards at Lucaston. We would like to thank Dr Michael Roach for assistance with the ERI, Garth Oliver, Justin Direen and Abbas Almajmaie for assistance with field work. This project has been funded by Horticulture Australia Ltd under the ‘Productivity, Irrigation, Pests and Soils’ (PIPS) program, using the apple and pear industry levy, voluntary contributions from the New Zealand Institute for Plant and Food Research, and matched funds from the Australian Government.

References

- Abramoff MD, Magelhaes PJ, Ram SJ (2004) Image processing with ImageJ. *Biophotonics Int* 11:36–42
- Algeo J, Van Dam RL, Slater L (2016) Early-time GPR: a method to monitor spatial variations in soil water content during irrigation in clay soils. *Vadose Zone J*. <https://doi.org/10.2136/vzj2016.03.0026>
- Alletto L, Coquet Y, Vachier P, Labat C (2006) Hydraulic conductivity, immobile water content, and exchange coefficient in three soil profiles. *Soil Sci Soc Am J* 70:1272–1280
- Bar-Yosef B, Schwartz S, Markovich T, Lucas B, Assaf R (1988) Effect of root volume and nitrate solution concentration on growth, fruit yield, and temporal N and water uptake rates by apple trees. *Plant Soil* 107:49–56
- BOM (2015) Climate statistics for Australian locations: Grove, Tasmania. Bureau of Meteorology. http://www.bom.gov.au/climate/averages/tables/cw_094069.shtml. Accessed Jan 2015
- Carrillo MLK, Letey J, Yates SR (2000) Unstable water flow in a layered soil: I. effects of a stable water-repellent layer. *Soil Sci Soc Am J* 64:450–455
- Cassiani G, Boaga J, Vanella D, Perri MT, Consoli S (2015) Monitoring and modelling of soil–plant interactions: the joint use of ERT, sap flow and eddy covariance data to characterize the volume of an orange tree root zone. *Hydrol Earth Syst Sci* 19:2213–2225. <https://doi.org/10.5194/hess-19-2213-2015>
- Cassiani G, Boaga J, Rossi M, Putti M, Fadda G, Majone B, Bellin A (2016) Soil–plant interaction monitoring: small scale example of an apple orchard in Trentino, North-eastern Italy. *Sci Total Environ* 543:851–861. <https://doi.org/10.1016/j.scitotenv.2015.03.113>
- Chittleborough DJ, Smettem KRJ, Kirkby C (1994) Clay, phosphate and water movement through a texture contrast soil. Land and Water Resource Research and Development Corporation, for Project UAD1, LWRRRC, Canberra
- Clothier B, Heng L, Magesan G, Vogeler I (1995) The measured mobile-water content of an unsaturated soil as a function of hydraulic regime. *Soil Res* 33:397–414 doi. <https://doi.org/10.1071/SR9950397>
- Clothier BE, Green SR, Deurer M (2008) Preferential flow and transport in soil: progress and prognosis. *Eur J Soil Sci* 59:2–13 <https://doi.org/10.1111/j.1365-2389.2007.00991.x>
- Consoli S, Stagno F, Vanella D, Boaga J, Cassiani G, Rocuzzo G (2017) Partial root-zone drying irrigation in orange orchards: effects on water use and crop production characteristics. *Eur J Agron* 82:190–202. <https://doi.org/10.1016/j.eja.2016.11.001>
- Cook FJ, Thorburn PJ, Fitch P, Bristow KL (2003) WetUp: a software tool to display approximate wetting patterns from drippers. *Irrig Sci* 22:129–134. <https://doi.org/10.1007/s00271-003-0078-2>
- Cook FJ, Fitch P, Thorburn PJ, Charlesworth PB, Bristow KL (2006a) Modelling trickle irrigation: comparison of analytical and numerical models for estimation of wetting front position with time. *Environ Model Softw* 21:1353–1359. <https://doi.org/10.1016/j.envsoft.2005.04.018>
- Cook FJ, Jayawardane NS, Rassam DW, Christen EW, Hornbuckle JW, Stirzaker RJ, Bristow KL, Biswas TK (2006b) The state of measuring, diagnosing, ameliorating and managing solute effects in irrigated systems. Technical Report No. 04/06, CRC for Irrigation Futures
- Coppola A et al (2016) Calibration of an electromagnetic induction sensor with time-domain reflectometry data to monitor rootzone electrical conductivity under saline water irrigation. *Eur J Soil Sci* 67:737–748. <https://doi.org/10.1111/ejss.12390>
- Cotching WE, Lynch S, Kidd DB (2009) Dominant soil orders in Tasmania: distribution and selected properties. *Soil Res* 47:537–548. <https://doi.org/10.1071/SR08239>
- Cote CM, Bristow KL, Charlesworth PB, Cook FJ, Thorburn PJ (2003) Analysis of soil wetting and solute transport in subsurface trickle irrigation. *Irrig Sci* 22:143–156
- Dekker LW, Ritsema CJ (1996) Uneven moisture patterns in water repellent soils. *Geoderma* 70:87–99
- Devasirvatham V (2009) A review of subsurface drip irrigation in vegetable production, vol CRC. Irrigation futures irrigation matters series no. 03/09. CRC for Irrigation Futures
- Durner W (1994) Hydraulic conductivity estimation for soils with heterogeneous pore structure. *Water Resour Res* 30:211–223
- Eastham J, Gregory PJ, Williamson DR (2000) A spatial analysis of lateral and vertical fluxes of water associated with a perched watertable in a duplex soil. *Austr J Soil Res* 38:879–890
- El-Nesr MN, Alazba AA, Šimůnek J (2014) HYDRUS simulations of the effects of dual-drip subsurface irrigation and a physical barrier on water movement and solute transport in soils. *Irrig Sci* 32:111–125. <https://doi.org/10.1007/s00271-013-0417-x>
- FAO (1997) Small-scale irrigation for arid zones. Principles and options. Food and Agriculture Organisation of the United Nations (FAO), Rome
- Flury M, Fluhler H, Jury WA, Leuenberger J (1994) Susceptibility of soils to preferential flow of water: a field study. *Water Resour Res* 30:1945–1954
- Furman A, Ferré TPA, Warrick AW (2003) A sensitivity analysis of electrical resistivity tomography array types using analytical element modeling. *Vadose Zone J* 2:416–423
- Gärdenäs AI, Hopmans JW, Hanson BR, Šimůnek J (2005) Two-dimensional modeling of nitrate leaching for various fertigation scenarios under micro-irrigation. *Agric Water Manag* 74:219–242. <https://doi.org/10.1016/j.agwat.2004.11.011>
- Gerke HH, Germann P, Nieber J (2010) Preferential and unstable flow: from the pore to the catchment scale. *Vadose Zone J* 9:207–212. <https://doi.org/10.2136/vzj2010.0059>
- Golden Software (2002) Surfer user guide: contouring and 3D surface mapping for scientists and engineers. Colorado
- Goldy R (2012) Soil type influences irrigation strategy. Michigan State University extension. http://msue.anr.msu.edu/news/soil_type_influences_irrigation_strategy
- Han X et al (2016) Simultaneous soil moisture and properties estimation for a drip irrigated field by assimilating cosmic-ray neutron intensity. *J Hydrol* 539:611–624. <https://doi.org/10.1016/j.jhydrol.2016.05.050>
- Hardie MA, Cotching WE, Doyle RB, Holz G, Lissos S, Mattern K (2011) Effect of antecedent soil moisture on preferential flow in a texture-contrast soil. *J Hydrol* 398:191–201. <https://doi.org/10.1016/j.jhydrol.2010.12.008>
- Hardie MA, Mitchelson H, Doyle R (2012) Efficiency and efficacy of drip irrigation in a Tasmanian Vineyard Irrigation performance was determined by dye tracer staining, soil hydraulic assessment and modelling. In: Paper presented at the proceedings of the 5th joint soil science Australia and New Zealand society of soil science conference, Hobart, 2–7 Dec 2012

- Hardie M, Doyle R, Cotching W, Holz G, Lisson S (2013) Hydrogeology and preferential flow in the Tasmanian texture-contrast soils. *Vadose Zone J*. <https://doi.org/10.2136/vzj2013.03.0051>
- Hossain MB, Lamb DW, Lockwood PV, Frazier P (2010) EM38 for volumetric soil water content estimation in the root-zone of deep vertosol soils. *Comput Electron Agric* 74:100–109. <https://doi.org/10.1016/j.compag.2010.07.003>
- Hu H, Mao X, Barry DA, Liu C, Li P (2015) Modeling reactive transport of reclaimed water through large soil columns with different low-permeability layers. *Hydrogeol J* 23:351–364. <https://doi.org/10.1007/s10040-014-1187-0>
- Hung J (1995) Determination of emitter spacing and irrigation run time including plant root depth. In: Lamm FR (ed) *Microirrigation for a changing world: conserving resources/preserving the environment*. Proceedings of the fifth international microirrigation congress, Orlando, 2–6 Apr 1995. ASAE, St. Joseph, pp 292–296
- Isbell RF (2002) *The Australian soil classification, vol 4*. Australian soil and land survey series. CSIRO Publishing, Melbourne
- Jarvis NJ (2007) A review of non-equilibrium water flow and solute transport in soil macropores: principles, controlling factors and consequences for water quality. *Eur J Soil Sci* 58:523–546
- Kandelous MM, Šimůnek J (2010) Comparison of numerical, analytical, and empirical models to estimate wetting patterns for surface and subsurface drip irrigation. *Irrig Sci* 28:435–444. <https://doi.org/10.1007/s00271-009-0205-9>
- Klein I, Spieler G (1987) Fertigation of apples with nitrate or ammonium nitrogen under drip irrigation. II. Nutrient distribution in the soil 1. *Commun Soil Sci Plant Anal* 18:323–339
- Klein I, Levin I, Bar-Yosef B, Assaf R, Berkovitz A (1989) Drip nitrogen fertigation of ‘Starking delicious’ apple trees. *Plant Soil* 119:305–314. <https://doi.org/10.1007/bf02370423>
- Koestel J, Kasteel R, Kemna A, Esser O, Javaux M, Binley A, Vereecken H (2009) Imaging brilliant blue stained soil by means of electrical resistivity tomography. *Vadose Zone J* 8:963–975. <https://doi.org/10.2136/vzj2008.0180>
- Kowalenko CG, Yu S (1996) Assessment of nitrate adsorption in soils by extraction, equilibration and column-leaching methods. *Can J Soil Sci* 76:49–57
- Li X, Shi H, Šimůnek J, Gong X, Peng Z (2015) Modeling soil water dynamics in a drip-irrigated intercropping field under plastic mulch. *Irrig Sci* 33:289–302. <https://doi.org/10.1007/s00271-015-0466-4>
- Lipsius K, Mooney SJ (2006) Using image analysis of tracer staining to examine the infiltration patterns in a water repellent contaminated sandy soil. *Geoderma* 136:865–875
- Loke M (2010) RES2DINV ver 3.59 User Manual. Geotomo Software, Gelugor, Malaysia
- McKenzie NJ, Coughlan KL, Cresswell HP (2002) *Soil physical measurement and interpretation for land evaluation*. CSIRO Publishing, Melbourne
- Mguidiche A, Provenzano G, Douh B, Khila S, Rallo G, Boujelben A (2015) Assessing hydrus-2D to simulate soil water content (SWC) and salt accumulation under an SDI system: application to a potato crop in a semi-arid area of Central Tunisia. *Irrig Drain* 64:263–274. <https://doi.org/10.1002/ird.1884>
- Michot D, Benderitter Y, Dorigny A, Nicoulaud B, King D, Tabbagh A (2003) Spatial and temporal monitoring of soil water content with an irrigated corn crop cover using surface electrical resistivity tomography. *Water Resour Res* 39:SBH141–SBH1420
- Miller CR, Routh PS, Brosten TR, McNamara JP (2008) Application of time-lapse ERT imaging to watershed characterization. *Geophysics* 73:G7–G17. <https://doi.org/10.1190/1.2073888>
- Misra RK, Padhi J (2014) Assessing field-scale soil water distribution with electromagnetic induction method. *J Hydrol* 516:200–209. <https://doi.org/10.1016/j.jhydrol.2014.02.049>
- Mon J, Flury M (2005) Dyes as hydrological tracers. In: Lehr JH, Keeley J, Lehr J (eds) *Encyclopedia of water*. Wiley, New York
- Moreno Z, Arnon-Zur A, Furman A (2015) Hydro-geophysical monitoring of orchard root zone dynamics in semi-arid region. *Irrig Sci* 33:303–318. <https://doi.org/10.1007/s00271-015-0467-3>
- Naglič B, Kechavarzi C, Coulon F, Pintar M (2014) Numerical investigation of the influence of texture, surface drip emitter discharge rate and initial soil moisture condition on wetting pattern size. *Irrig Sci* 32:421–436. <https://doi.org/10.1007/s00271-014-0439-z>
- Nováková K, Nágel D (2009) The influence of irrigation on nitrates movement in soil and risk of subsoil contamination. *Soil Water Res* 4:S131–S136
- O’Dell J (1993) Method 353.2, Revision 2.0: Determination of nitrate-nitrite nitrogen by automated colorimetry. Environmental Monitoring Systems Laboratory, U.S. Environmental Protection Agency, Cincinnati, Ohio
- Persson M, Dahlin T, Günther T (2015) Observing solute transport in the capillary fringe using image analysis and electrical resistivity tomography in laboratory experiments. *Vadose Zone J*. <https://doi.org/10.2136/vzj2014.07.0085>
- Peters A, Durner W (2008) Simplified evaporation method for determining soil hydraulic properties. *J Hydrol* 356:147–162
- Phogat V, Skewes MA, Cox JW, Alam J, Grigson G, Šimůnek J (2013) Evaluation of water movement and nitrate dynamics in a lysimeter planted with an orange tree. *Agric Water Manag* 127:74–84. <https://doi.org/10.1016/j.agwat.2013.05.017>
- Phogat V, Skewes MA, Cox JW, Sanderson G, Alam J, Šimůnek J (2014) Seasonal simulation of water, salinity and nitrate dynamics under drip irrigated mandarin (*Citrus reticulata*) and assessing management options for drainage and nitrate leaching. *J Hydrol* 513:504–516. <https://doi.org/10.1016/j.jhydrol.2014.04.008>
- Puy A, García Avilés JM, Balbo AL, Keller M, Riedesel S, Blum D, Bubbenzer O (2016) Drip irrigation uptake in traditional irrigated fields: the edaphological impact. *J Environ Manag*. <https://doi.org/10.1016/j.jenvman.2016.07.017>
- Rayment GE, Higginson FR (1992) *Australian laboratory handbook of soil and water chemical methods*. Australian soil and land survey handbook. Inkata Press, Melbourne
- Ritsema CJ, Dekker LW, Nieber JL, Steenhuis TS (1998) Modeling and field evidence of finger formation and finger recurrence in a water repellent sandy soil. *Water Resour Res* 34:555–567
- Roth K (2008) Scaling of water flow through porous media and soils. *Eur J Soil Sci* 59:125–130. <https://doi.org/10.1111/j.1365-2389.2007.00986.x>
- Samouëlian A, Cousin I, Tabbagh A, Bruand A, Richard G (2005) Electrical resistivity survey in soil science: a review. *Soil Tillage Res* 83:173–193
- Satriani A, Loperte A, Soldovieri F (2015) Integrated geophysical techniques for sustainable management of water resource. A case study of local dry bean versus commercial common bean cultivars. *Agric Water Manag* 162:57–66. <https://doi.org/10.1016/j.agwat.2015.08.010>
- Shamir O, Goldshleger N, Basson U, Reshef M (2016) Mapping spatial moisture content of unsaturated agricultural soils with ground-penetrating radar. *International archives of the photogrammetry, remote sensing and spatial information sciences—ISPRS archives*, pp 1279–1285. <https://doi.org/10.5194/isprsarchives-XLI-B8-1279-2016>
- Sheng F, Liu H, Wang K, Zhang R, Tang Z (2014) Investigation into preferential flow in natural unsaturated soils with field multiple-tracer infiltration experiments and the active region model. *J Hydrol* 508:137–146. <https://doi.org/10.1016/j.jhydrol.2013.10.048>
- Šimůnek J, van Genuchten MT (2007) Chap. 22: contaminant transport in the unsaturated zone: theory and modelling. In: Delleur JW (ed)

- The handbook of groundwater engineering, 2nd edn. CRC Press, Boca Raton, pp 22.21–22.38
- Šimůnek J, Jarvis NJ, van Genuchten MT, Gardenas A (2003) Review and comparison of models for describing non-equilibrium and preferential flow and transport in the vadose zone. *J Hydrol* 272:14–35
- Šimůnek J, van Genuchten MT, Šejna M (2008) Development and applications of the HYDRUS and STANMOD software packages and related codes. *Vadose Zone J* 7:587–600
- Šimůnek J, Van Genuchten MT, Šejna M (2012) Hydrus: model use, calibration, and validation. *Trans ASABE* 55:1261–1274
- Šimůnek J, Jacques D, Langergraber G, Bradford SA, Šejna M, Van Genuchten MT (2013) Numerical modeling of contaminant transport using HYDRUS and its specialized modules. *J Indian Inst Sci* 93:265–284
- Šimůnek J, van Genuchten MT, Šejna M (2016) Recent developments and applications of the HYDRUS computer software packages. *Vadose Zone J*. <https://doi.org/10.2136/vzj2016.04.0033>
- Smethurst PJ, Petrone KC, Langergraber G, Baillie CC, Worledge D, Nash D (2014) Nitrate dynamics in a rural headwater catchment: measurements modelling. *Hydrol Process* 28:1820–1834. <https://doi.org/10.1002/hyp.9709>
- Souza CF, Folegatti MV (2008) Characterization spatial and temporal patterns of water and solute distribution. *American Society of Agricultural and Biological Engineers. Annual international meeting 2008, ASABE 2008.*, pp 2327–2339
- Subbaiah R (2013) A review of models for predicting soil water dynamics during trickle irrigation. *Irrig Sci* 31:225–258. <https://doi.org/10.1007/s00271-011-0309-x>
- Thorburn PJ, Cook FJ, Bristow KL (2003) Soil-dependent wetting from trickle emitters: implications for system design and management. *Irrig Sci* 22:121–127. <https://doi.org/10.1007/s00271-003-0077-3>
- Ticehurst JL, Cresswell HP, McKenzie NJ, Glover MR (2007) Interpreting soil and topographic properties to conceptualise hillslope hydrology. *Geoderma* 137:279–292
- UMS (2013) HYPROP user manual. UMS GmbH München, Art. no. HYPROP
- van der Laan M, Annandale JG, Bristow KL, Stirzaker RJ, Du Preez CC, Thorburn PJ (2014) Modelling nitrogen leaching: are we getting the right answer for the right reason? *Agric Water Manag* 133:74–80. <https://doi.org/10.1016/j.agwat.2013.10.017>
- Wang Z, Feyen J, Nielsen DR, Van Genuchten MT (1997) Two-phase flow infiltration equations accounting for air entrapment effects. *Water Resour Res* 33:2759–2767
- Wang Z, Feyen J, Ritsema CJ (1998a) Susceptibility and predictability of conditions for preferential flow. *Water Resour Res* 34:2169–2182
- Wang Z, Feyen J, van Genuchten MT, Nielsen DR (1998b) Air entrapment effects on infiltration rate and flow instability. *Water Resour Res* 34:213–222
- Wang Z, Wu L, Wu QJ (2000a) Water-entry value as an alternative indicator of soil water-repellency and wettability. *J Hydrol* 231–232:76–83
- Wang Z, Wu QJ, Wu L, Ritsema CJ, Dekker LW, Feyen J (2000b) Effects of soil water repellency on infiltration rate and flow instability. *J Hydrol* 231–232:265–276
- Wang Z, Li J, Li Y (2014) Simulation of nitrate leaching under varying drip system uniformities and precipitation patterns during the growing season of maize in the North China Plain. *Agric Water Manag* 142:19–28. <https://doi.org/10.1016/j.agwat.2014.04.013>
- Wehrer M, Slater LD (2015) Characterization of water content dynamics and tracer breakthrough by 3-D electrical resistivity tomography (ERT) under transient unsaturated conditions. *Water Resour Res* 51:97–124. <https://doi.org/10.1002/2014WR016131>
- Wendroth O, Ehlers W, Hopmans JW, Kage H, Halbertsma J, Wosten JHM (1993) Reevaluation of the evaporation method for determining hydraulic functions in unsaturated soils. *Soil Sci Soc Am J* 57:1436–1443
- Williams MR, Buda AR, Elliott HA, Hamlett J, Boyer EW, Schmidt JP (2014) Groundwater flow path dynamics and nitrogen transport potential in the riparian zone of an agricultural headwater catchment. *J Hydrol* 511:870–879. <https://doi.org/10.1016/j.jhydrol.2014.02.033>
- Yao TM, Hendrickx JMH (1996) Stability of wetting fronts in dry homogeneous soils under low infiltration rates. *Soil Sci Soc Am J* 60:20–28
- Zhu Z, Tan L, Gao S, Jiao Q (2014) Observation on soil moisture of irrigation cropland by cosmic-ray probe. *IEEE Geosci Remote Sens Lett* 12:472–476. <https://doi.org/10.1109/LGRS.2014.2346784>